

Measurement of parameters of scintillating bars with wavelength-shifting fibres and silicon photomultiplier readout for the SHiP Muon Detector

A. Montanari,^a N. Tosi,^a W. Baldini,^b A. Calcaterra,^c G. Lanfranchi,^c A. Saputi,^c A. Khotjantsev,^d Yu. Kudenko,^{d,e,f} V. Kurochka,^d A. Mefodiev,^d O. Mineev^d

^a*INFN - Sezione di Bologna, Viale Berti Pichat, 6/2, 40127 Bologna, Italy*

^b*INFN - Sezione di Ferrara, via Saragat 1, 44122 Ferrara, Italy*

^c*INFN - Laboratori Nazionali di Frascati, via E. Fermi 40, 00044 Frascati (Rome), Italy*

^d*Institute for Nuclear Research of the Russian Academy of Science,
pr. 60-letiya Oktyabrya 7a, Moscow, Russia 117312*

^e*Moscow Institute of Physics and Technology, Institutskiy per. 9, Dolgoprudny, Moscow region,
Russia, 141701*

^f*National Research Nuclear University MEPhI, Kashirskoe sh. 31, Moscow, Russia, 115409*

E-mail: Gaia.Lanfranchi@lnf.infn.it

ABSTRACT: The light yield and the time resolution of different types of 3 m long scintillating bars instrumented with wavelength shifting fibres and read out by different models of silicon photomultipliers have been measured at a test beam at the T9 area at the CERN Proton Synchrotron. The results obtained with different configurations are presented. A time resolution better than 800 ps, constant along the bar length within 20%, and a light yield of ~ 140 (70) photoelectrons are obtained for bars 3 m long, ~ 4.5 (5) cm wide and 2 (0.7) cm thick. These results nicely match the requirements for the Muon Detector of the SHiP experiment.

KEYWORDS: Scintillators, scintillation and light emission processes (solid, gas and liquid scintillators); Photon detectors for UV, visible and IR photons (solid-state) (PIN diodes, APDs, Si-PMTs, G-APDs, CCDs, EBCCDs, EMCCDs etc);

Contents

1	Introduction	1
2	The prototypes	2
3	The photosensors	4
4	The beam line	4
5	The experimental setup	5
6	Results	6
6.1	Light yield and attenuation length	6
6.2	Detection efficiency	11
6.3	Time resolution	12
7	Conclusions	18

1 Introduction

Extruded plastic scintillator bars with wavelength shifting (WLS) fibres and Silicon Photomultiplier (SiPM) readout are considered an established technology for massive tracking calorimeters in long-baseline neutrino oscillation experiments. The MINOS experiment [1] uses extruded scintillator bars of $(1 \times 4.1 \times 800)$ cm³ size with 9 m long WLS fibres. A fine-grained detector in the *Minerva* experiment [2] employs triangular-shaped 3.5 m long strips and WLS fibres of 1.2 mm diameter. Other experiments that use the same technology are Belle II [3] and T2K [4]. This technology has been considered also as a viable option for the muon system of the SHiP experiment [5] proposed at the CERN SPS. The SHiP muon detector comprises four muon stations interleaved by iron filters, each station with a transverse dimension of (6×12) m² for a total active area of 288 m². Each station has to provide both spatial and time information. The x, y coordinate will be obtained by the crossing of horizontal and vertical bars 3 m long, with a granularity to be defined between 5 and 10 cm. The time information is provided by the average of the times measured at both ends of the bars. A time resolution better than 1 ns per station is required. This paper shows the results obtained on different types of extruded scintillating bars instrumented with different types of WLS fibres and SiPMs measured at a test beam held at the T9 area of the CERN Proton Synchrotron (PS) in the period October 14-28, 2015.

2 The prototypes

Given the relatively large area, a good choice for the SHiP Muon system is the rather inexpensive scintillators produced at the FNAL-NICADD facility [6, 7] which are fabricated by co-extrusion with a thin layer of TiO_2 around the active core. Another possibility is the polystyrene scintillator bars extruded at UNIPLAST plant (Vladimir, Russia) [8].

Since the attenuation length of the plastic scintillator is rather short, the light produced by the particle interaction has to be collected, re-emitted, and transported to the photodetectors efficiently by WLS fibres. These fibres need to have a good light yield to ensure a high detection efficiency for fibre lengths of ~ 3 m. Possible choices for WLS fibres are those produced by Saint-Gobain [9] and from Kuraray [10] factories. Both companies produce multicladding fibres with long attenuation length (~ 4 m) and good trapping efficiency ($\sim 5\%$). The fibres from Kuraray have a higher light yield while Saint-Gobain fibres have a faster response (~ 2.7 ns versus ~ 10 ns of the Kuraray), which ensures a better time resolution for the same light yield.

Scintillating bars from NICADD and UNIPLAST companies of different lengths, widths and thicknesses were instrumented with different types and numbers of WLS fibres from Kuraray and Saint-Gobain manufacturers and read out by different types of SiPMs from Hamamatsu and AdvanSiD (FBK) companies.

Table 1 and Table 2 show the main parameters of scintillating bars from NICADD and Uniplast manufacturers, respectively.

Table 1. Prototypes of extruded scintillator bars from NICADD manufacturer. All the bars were instrumented with fibres Kuraray WLS Y11(200) S-type except the S2 bar that has been instrumented with fibres from the Saint Gobain company (BCF92). The fibres in the L1, L2 and L4 bars were read out at both ends. The fibres in the S1, S2, S5 and S8 bars were read out only at one end. The main parameters of the photosensors are shown in Table 3.

	Bar dimensions ($h \times w \times l$) mm 3	number of fibres/bar	fibre diameter [mm]	SiPM model (AdvanSiD company)
L1	($10 \times 45 \times 3000$) mm 3	1 fibre in 1 groove	2	ASD-NUV3S-P
L2	($20 \times 40 \times 3000$) mm 3	1 fibre in 1 groove	2	ASD-NUV3S-P
L4	($20 \times 40 \times 3000$) mm 3	1 fibre in 1 groove	1.2	ASD-NUV1S-P
S1	($10 \times 45 \times 250$) mm 3	2 fibres in 1 groove	1.2	ASD-NUV3S-P
S2	($10 \times 45 \times 250$) mm 3	2 fibres in 1 groove	1.2	ASD-NUV3S-P
S5	($20 \times 40 \times 250$) mm 3	2 fibres in 1 groove	1.2	ASD-NUV3S-P
S8	($20 \times 40 \times 250$) mm 3	1 fibre in 1 hole	2	ASD-NUV3S-P

The L1, L2 and L4 prototypes from NICADD company are 3 m long, of different widths and thicknesses as shown in Table 1. These bars were machined with a single straight groove, on the top face, to host 1.2 mm or 2 mm diameter Kuraray Y11 (S300) fibres. The S1, S2, S5 and S8 are 25 cm long bars, of different widths and thicknesses, and were used to test different configurations with two fibres hosted in the same groove or one fibre hosted in a hole machined at the center of the bar. These bars were read out only at one end. The

Table 2. Prototypes of extruded scintillating bars from UNIPLAST manufacturer. All the bars were instrumented with fibres Kuraray WLS Y11(200) S-type. In the bars U1, U2 and U3 the fibres were read out at both ends, in the U4 bar the two fibres were read out just at one end, opposite with respect to each other. The main parameters of the photosensors are shown in Table 3.

	Bar dimensions (h × w × l) mm ³	number of fibres/bar	fibre diameter [mm]	SiPM model (Hamamatsu company)
U1	(7 × 30 × 3000) mm ³	1 fibre in 1 groove	1	MPPC S13081-050CS
U2	(7 × 50 × 3000) mm ³	1 fibre in 1 groove	1	MPPC S13081-050CS
U3	(7 × 100 × 3000) mm ³	2 fibres in 2 grooves	1	MPPC S13081-050CS
U4	(7 × 100 × 3000) mm ³	2 fibres in 2 grooves	1	MPPC S13081-050CS

fibres were all fixed with BC-600 optical cement from Saint-Gobain company. An adhesive aluminum tape has been applied on top of the grooves to reflect the light emerging from the groove. The photosensors used for NICADD bars are ASD-NUV3S-P or ASD-NUV1S-P from the AdvanSiD company [11] whose main parameters are listed in Table 3.

The 3 m long U1, U2, U3 and U4 prototypes of 0.7 cm thickness were extruded at the Uniplast Factory (Vladimir, Russia) and then cut to the 3, 5 and 10 cm wide bars. The scintillator composition is a polystyrene doped with 1.5% of paraterphenyl (PTP) and 0.01% of POPOP. The bars were covered by a chemical reflector by etching the scintillator surface in a chemical agent that results in the formation of a white micropore deposit over a polystyrene [13]. The chemical coating is an excellent reflector, besides it dissolves rough surface acquired during the cutting process. A 2 mm deep and 1.1 mm wide groove has been machined along a bar central line in 3 and 5 cm wide bars to accomodate a WLS fibre. The 10 cm wide bars have two grooves running 5 cm apart. The fibres of all prototypes are read out at both ends except for the U4 bar where each fiber is read out only at one end. The four prototypes of the UNIPLAST bars are sketched in Figure 1.

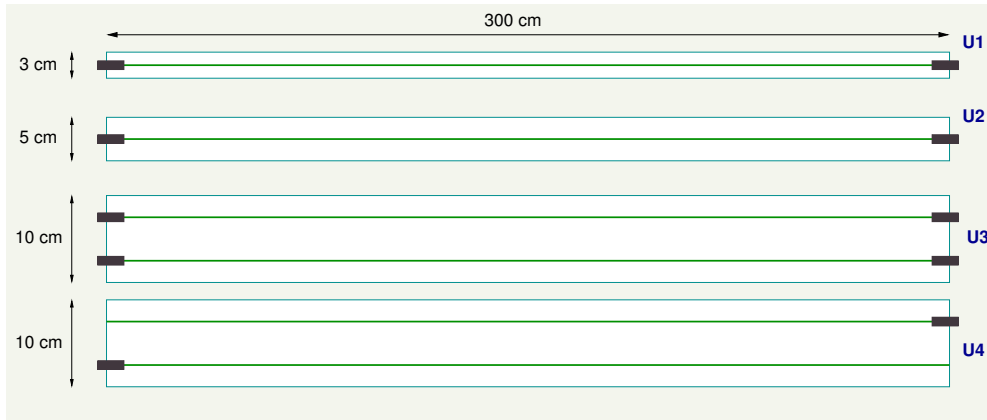


Figure 1. Four types of bars manufactured at Uniplast factory.

The fibres of one of the 10 cm wide bars (U4) have been read out only at one end

in such a way that the bar is viewed from both ends only by two photosensors, one per fibre. The fibres used for UNIPLAST bars are Kuraray WLS Y11 multi-clad fibres of 1 mm diameter. The glue used to couple the fibres with a scintillator is optical cement EJ500 from Eljen Technology [14]. The same glue has been used to embed optical connectors into the groove. The plastic optical connector consists of two parts: a ferrule part glued into the scintillator and a container to hold a Hamamatsu MPPC SiPM. Both parts are latched by a simple snap-like mechanism. A foam spring inside the container provides reliable optical contact between the photosensor and the fibre end.

3 The photosensors

Bars from NICADD and Uniplast manufacturers are read out by photosensors from AdvanSiD and Hamamatsu companies, respectively. The main parameters of the photosensors are shown in Table 3. Uniplast bars were instrumented with low crosstalk Hamamatsu MPPC S13081-050CS [15] with sensitive area size of $(1.3 \times 1.3) \text{ mm}^2$. NICADD bars were instrumented with ASD-NUV3S-P [16] and ASD-NUV1S-P [17] with squared area of dimensions $(3 \times 3) \text{ mm}^2$ and circular area of 1.2 mm diameter, respectively.

Table 3. Parameters of SiPMs from different manufacturers.

Parameter	Hamamatsu MPPC S13081-050CS	AdvanSiD ASD -NUV3S-P
Pixel size, μm	50	40
Number of pixels	667	5520
Sensitive area, mm^2	1.3×1.3	3.0×3.0
Gain	1.5×10^6	2.6×10^6 (at +4 V over-voltage)
Dark rate, kHz/mm^2 (at $T=300 \text{ K}$)	~ 90	< 100
Crosstalk, %	~ 1	~ 25 (at +4 V over-voltage)
PDE	$\sim 33\%$ at 520 nm	25% at 520 nm
Voltage bias, V	70 V at $T = 23 \text{ }^\circ\text{C}$	30 V at $T = 23 \text{ }^\circ\text{C}$

4 The beam line

The T9 beam at the CERN PS is a secondary beam line produced from a 24 GeV/c primary proton beam slowly extracted from the PS. The line transports either positive or negative particles in the momentum range between 0.5 and 10 GeV/c and with a momentum resolution of $\sim 0.5\%$. The beam is a mixed particle beam. Depending on the beam momentum and charge chosen there are pions, (anti)-protons, e^+ or e^- and, at the percent level, also kaons and muons. For the negatively charged beam, the fraction of electrons can be as high as 80% for $p = 0.5 \text{ GeV/c}$ but drops to 5% at 5 GeV/c, for the “electron-enriched” target and to few per mille when the “hadron-enriched” target is used. The maximum particle

rate per burst of 10^6 is achieved for a $p = 10$ GeV/c positive beam. For negative beams the rates are typically 2-3 times lower and drop significantly at lower energy. The beam is delivered uniformly over a burst of 0.4 seconds. Depending on scheduling such a burst is provided typically once or twice every ~ 15 seconds.

A negative charged beam with momentum of 10 GeV/c produced with a “hadron-enriched” target has been used for the measurements discussed in this paper. This choice allows us to have a beam dominated by minimum ionizing particles (mip) and to minimize the fraction of electrons showering in the material of the experimental setup. A trigger rate of $\mathcal{O}(100$ Hz) has been obtained by closing the beam collimators, in order to maximize the fraction of single-hit events.

5 The experimental setup

Bars from NICADD and Vladimir companies were tested simultaneously using a common trigger made of two scintillators of $(13 \times 5 \times 1)$ cm 3 dimensions read out by photomultipliers, put in cross one in front and the other behind the bars, and selecting an active rectangular area of (1×5) cm 2 . Bars from different companies were read out by independent, similar setups as described below. In both setups the signals were read out by digitizers which record the full signal waveforms. This information will be also used for design of the front-end electronics (FEE) for the muon system of the SHiP experiment.

The experimental setup for NICADD bars is described in the following paragraph. The coincidence of the two scintillators has been used to start the readout of a buffer of a 10-bit, 8 (4) channels, 1 (2) GS/s VME digitizer CAEN V1751. One of the two trigger scintillator signals has been sent to the digitizer for time reference. Signals from the SiPMs were sent via 4 m long RG-174 cables to a 8-channels, 350 MHz bandwidth, 20 db gain, custom preamplifier board based on AD8000 current feedback operational amplifier and then to the digitizer. A VME interface has been used to send the data to a PC in the control room via a 30 m long optical fibre.

The signal charge has been measured by integrating the signal waveform within 350 ns window. In order to express the light yield in number of photoelectrons (p.e.), the integrated charge spectra corresponding to dark noise events were registered on a scope and used to extract the calibration constants for SiPMs. In fact, thanks to the high level of crosstalk ($\sim 25\%$) of the SiPM from the AdvanSiD company, up to three single photoelectron peaks were clearly visible even in dark noise events and used to evaluate the charge corresponding to one photoelectron. A global uncertainty of 3% has been associated to the calibration constants, taking into account the fitting procedure and the effect for temperature fluctuations (roughly 5 °C day/night). The optical crosstalk in the SiPMs has been statistically subtracted from the measured light yield.

For Uniplast bars, signals from the MPPCs were sent through a 2.5 m long twisted pair cable to a multi-channel custom made preamplifier with differential inputs. The differential inputs suppressed the electronic pickup noise in the experimental hall, nevertheless an additional screening has been required to obtain good separation between single photoelectron (p.e.) peaks in the MPPC charge spectra. After shielding the twisted pair wires with Al-foil

connected to ground, up to 20 p.e. peaks were visible in the charge spectrum. An example of the spectrum used for the calibration of the light yield is shown in Figure 2.

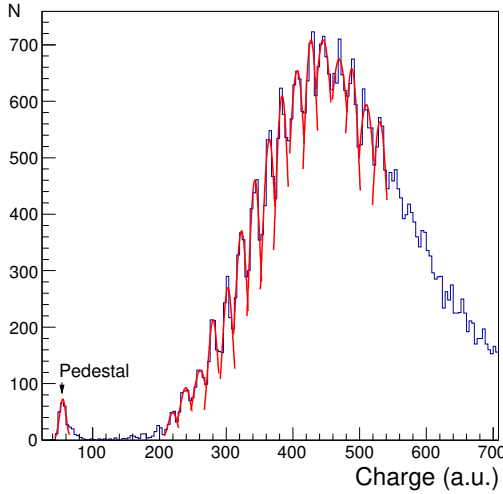


Figure 2. Example of spectrum used for the calibration of the light yield.

Then the signals were digitized by a 12-bit 5-GS/s switched capacitor desktop waveform digitizer CAEN DT5742. Six readout channels were operated simultaneously. The signal charge has been calculated by integrating the signal waveform within 200 ns window. The pulse rise time has been analyzed to obtain the timing parameters. The calibration of the MPPCs to express the light yield in number of p.e. has been done in the position where the beam hits a bar at the far end from the considered MPPC. The light output in this configuration was around 20 p.e. so 16 single p.e. peaks were averaged to obtain the calibration coefficients. The calibration coefficients were measured once. No corrections for temperature fluctuations (within roughly 5° C day/night) were made. This contributes to the systematic uncertainty of the light yield measured from data collected over a few days. The specified value of optical crosstalk in the Hamamatsu MPPCs is about 1% and this factor has been neglected in the light yield determination.

6 Results

6.1 Light yield and attenuation length

The light yield for NICADD bars has been obtained by measuring the light yields at both ends of 3 m long bars and at one end for 25 cm long bars. An example of the light yield distribution is shown in Figure 3. The spectrum is fitted with a Gaussian plus a Landau function with common mean and sigma values. The mean value and its uncertainty obtained from the fit are used to determine the light yield and its uncertainty for a given beam position.

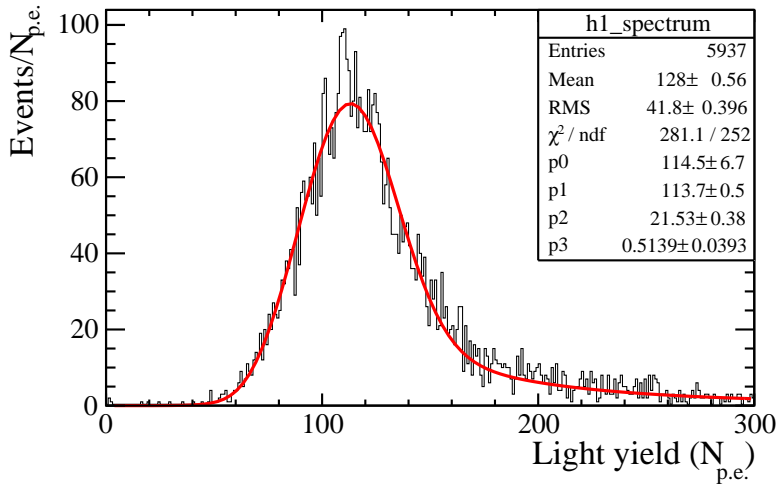


Figure 3. Example of light yield distribution for 2 cm thick NICADD bars.

For long bars, the attenuation of the light during the propagation along the fibre has been determined by measuring the light yield as a function of the distance of the beam from each photosensor. To perform this measurement the bar has been moved with respect to the trigger position by 25 cm steps. The results are shown in Figures 4, 5 and 6 for bars L1, L2, and L4, respectively. The attenuation behaviour of the Y11 fibre shows two components, an initial strong attenuation over a distance of about ~ 25 cm, probably dominated by the absorption in the fibre cladding, followed by a much longer attenuation length ($\lambda \sim 4.5 - 5$ m). This is consistent with previously published data [12].

The total light yield measured at both ends is constant within 20% along the bar. Figure 7 shows the total light yield for the three long bars from the NICADD company.

Table 4 shows the light yield measured at one end of the short bars S1,S2,S5 and S8 (as defined in Table 1) when the beam impinges at ~ 13 cm far from the SiPM. As comparison, the light yield measured at one end for long bars is also shown for the same beam position. The highest light yield is measured for the S5 bar, which is 2 cm thick with two Kuraray fibres, 1.2 mm diameter each, embedded in the same groove. The comparison of the results obtained with S1 and S2 bars shows that the Bicron fibres emit about half of the light produced by Kuraray fibres with the same diameter. Another interesting result is that a fibre glued in a groove on the top face of the scintillator bar (L2) produces the same amount of light of the same fibre glued in a hole in the middle of the bar (S8). In general, the light collected and re-emitted by a fibre is proportional to the transverse area of the fibre itself (we measured about a factor three more light produced by a fibre of 2 mm diameter (L2) with respect to a fibre of 1.2 mm diameter (L4)) while the light yield obtained by doubling the thickness of the scintillator is only 30% more (L2 versus L1).

The light yield for Uniplast bars has been measured by using three samples of 3 cm wide bars (U1), three samples of 5 cm wide bars (U2) and single prototypes of 10 cm wide bars (U3 and U4). Figure 8 shows the average result for all three tested bars of the same

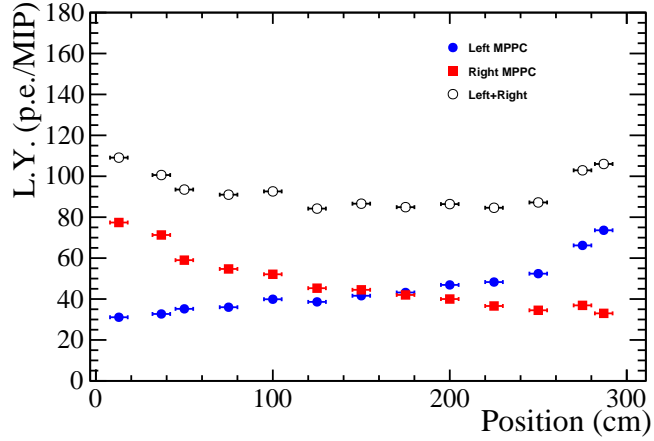


Figure 4. L1 bar: light yield measured at each end (red squares and blue solid circles) and the sum of the light yields at both ends (black open circles) as a function of the incident beam position along the bar.

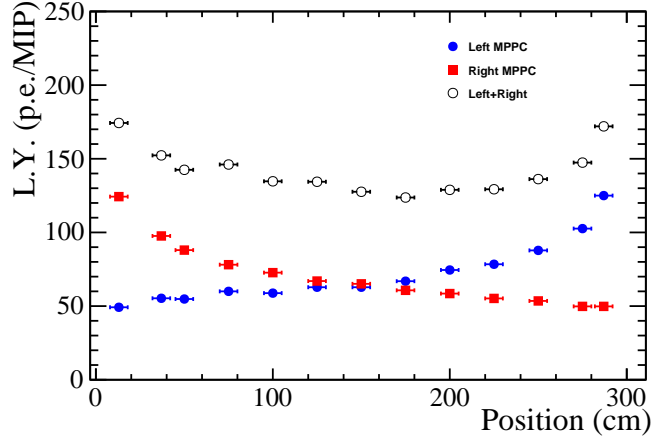


Figure 5. L2 bar: light yield measured at each end (red squares and blue solid circles) and the sum of the light yields measured at both ends (black open circles) as a function of the incident beam position along the bar.

width. The position of the bar with respect to the beam has been changed in steps 10 cm each, collecting 29 points altogether.

Scan results are shown in Figure 8 for 3 cm (U1) and 5 cm (U2) wide bars. The total light yield from both ends has been measured to be about 60 and 50 p.e. per minimum ionizing particle (MIP) for U1 and U2 respectively, when the beam impinges at the center of the bars. The light yield is higher by 20% when the beam impinges near the ends.

Figure 9 shows the scan results for 10 cm wide bars, U3 type (left) and U4 (right), respectively. For U3 bars, the total light yield from all 4 MPPCs is about 45 p.e./MIP when the beam impinges at the center of the bars. Plot on the right shows the light yield for the bar U4, where two WLS fibres are read out by two MPPCs, one per fibre at opposite

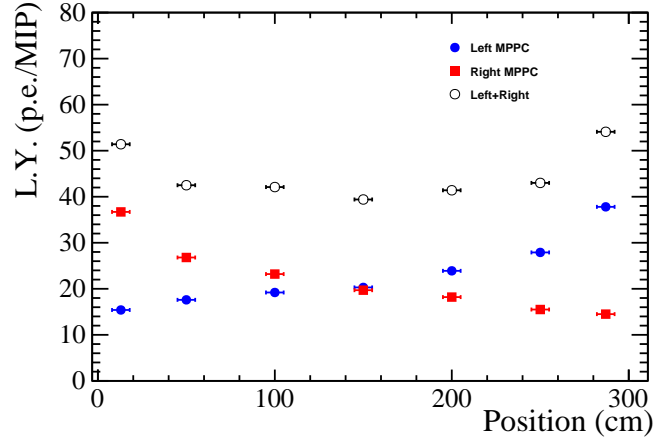


Figure 6. L4 bar: light yield measured at each end (red squares and blue solid circles) and the sum of the light yields measured at both ends (black open circles) as a function of the beam position along the bar.

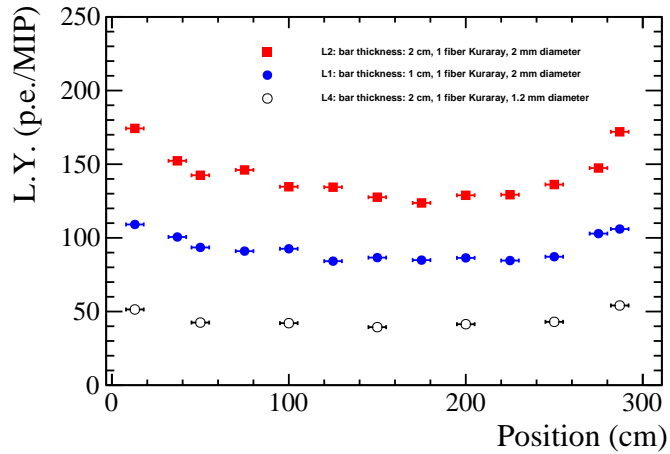


Figure 7. Sum of the light yield measured at each as a function of the beam position along the bar for L2, L1, L4 bar.

bar ends. This configuration gives the total light output of about 27 p.e./MIP in the center.

The scan has been also performed in the transverse dimension of the bar, to investigate how the light yield depends in the distance between the hit point and the WLS fibre. This scan was done with the beam impinging in the middle of the bar length. Bars 3, 5 and 10 cm wide were tested, with a single fibre read out at both ends. Only events selected by a (3×3) mm 2 area small plastic counter read out by a MPPC in the same way as the bars under test were considered.

The results are shown in Figure 10 (a). The first point of the scan was arbitrary fixed near the bar edges. The scan spanned over 5 cm towards the opposite edge crossing a fibre position at the coordinate of around 20–25 mm. The light yield is the sum of the light measured by the two photosensors at both ends of the bar. The attenuation of the

Table 4. Light yield measured at one end of the short bars S1,S2,S5 and S8 defined in Table 1 when the beam impinges at ~ 13 cm far from the SiPM. For comparison of different prototypes, the light yield measured at one end for long bars is also shown for the same beam position. The higher light yield is measured for the S5 bar. The uncertainty is dominated by the systematic one.

	light yield [p.e./MIP]
S1	78.0 ± 2.3
S2	41.0 ± 1.2
S5	133.0 ± 4.0
S8	105.9 ± 3.2
L1	77.4 ± 2.3
L2	114.3 ± 3.4
L4	36.7 ± 1.1
U1	50.7 ± 1.2
U2	45.3 ± 1.2
U3	22.3 ± 0.6
U4	19.8 ± 0.6

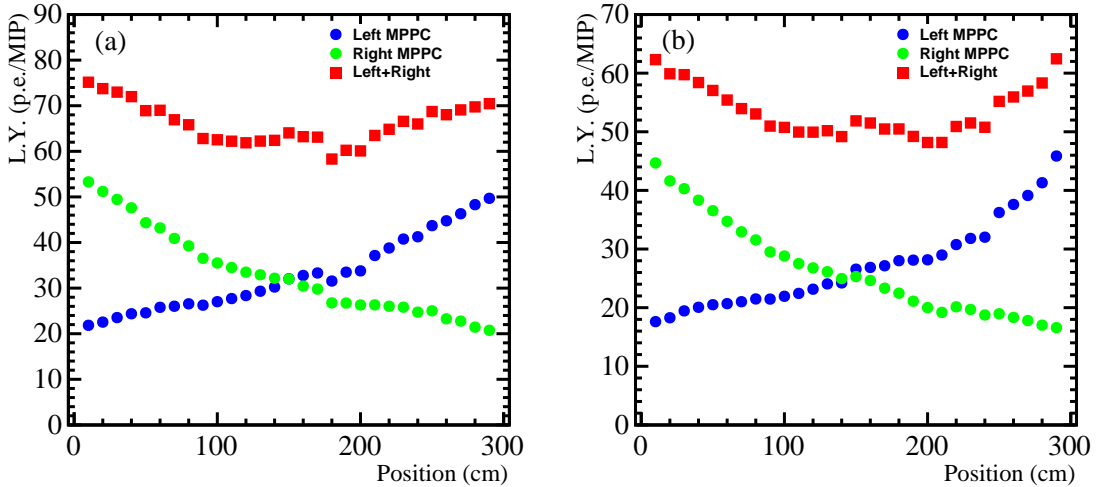


Figure 8. Light yield scan for 3 cm bars U1 (a) and 5 cm bars U2 (b).

scintillating light in the opposite directions from a fibre is demonstrated in Figure 10 (b) for the 10 cm wide bar. Light attenuation is asymmetrical because of the effect of close reflective edge in one direction. The points were fitted with exponential function $f(x) = C \cdot \exp(S \cdot x)$, where x is the position variable and attenuation length is $1/S$. An attenuation length of 76 mm has been obtained towards the near edge, and 49 mm in the opposite direction, where the edges influence on the scintillating light collection is less important. The second value can be considered to a first approximation as the attenuation length of scintillating light propagation in 7 mm thick extruded scintillator.

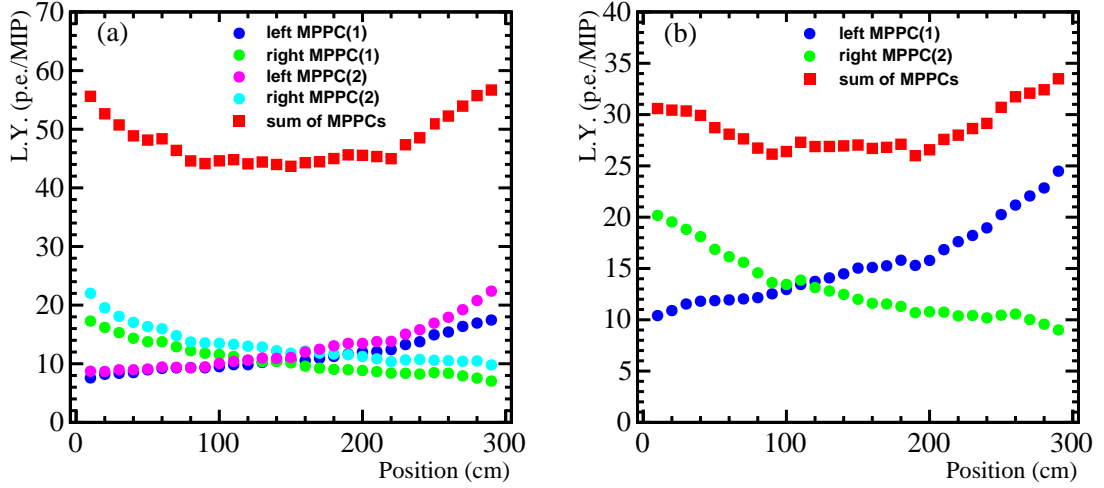


Figure 9. Light yield scan for 10 cm bars U3 (a) and U4 (b).

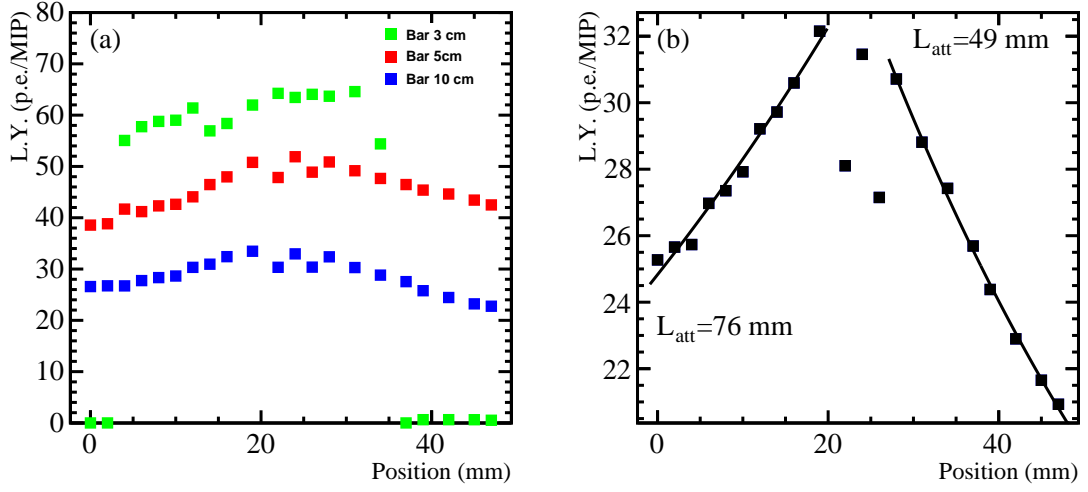


Figure 10. Light yield scan across 3 cm, 5 cm and 10 cm bars (a). Attenuation of scintillating light in the opposite directions from a fibre in the 10 cm bar (b).

6.2 Detection efficiency

Data obtained during the scan measurements across the bars have been used to calculate the detection efficiency. The electronic trigger signal was produced by two trigger counters in coincidence. An additional trigger counter of $3 \times 3 \text{ mm}^2$ active area allowed us to localize the position of the impinging beam on the tested bars with high accuracy. Only data collected with the beam impinging far from the bar edges have been considered for this measurement. Events with the signals from the small counter with a pulse amplitude

higher than 10 p.e. and time coordinate within $\pm 4\sigma_t$ with respect to the average time were selected for measuring the detection efficiency.

The detection efficiency has been obtained with three different methods:

1. as the ratio between the number of hits within $4\sigma_t$ of the $(t_L - t_R)/2$ spectrum and the total number of triggers, where t_L and t_R are the times measured from the SiPMs situated at the left and right bar end with respect to the direction of the beam (*timing AND*);
2. as the ratio between the number of hits within $4\sigma_t$ of the time distribution of one of the two photosensors and the total number of triggers (*timing OR*);
3. as the ratio between the number of hits with an integrated charge over some threshold at both bar ends and the total number of triggers (*charge AND*).

The *timing AND* method implies the most stringent selection criterion while the *timing OR* depends on the noise level of the photosensors. The *charge AND* method is the loosest criterion and it is affected by accidentals within 200 ns charge integration window.

The results are listed in Table 5 for the three methods and for 3, 5 and 10 cm wide bars. The 10 cm wide bar was read out by a single fibre at both ends. Only signals with more than 3 p.e. at each bar end have been considered in the analysis.

Table 5. Detection inefficiency for different prototypes and for different methods of counting the detected events. The uncertainty is purely statistical.

Method of counting	(1- ε) (%)	(1- ε) (%)	(1- ε) (%)
	width = 3 cm	width = 5 cm	width = 10 cm
Timing AND	0.32 \pm 0.03	0.26 \pm 0.02	0.59 \pm 0.04
Timing OR	0.27 \pm 0.03	0.13 \pm 0.02	0.09 \pm 0.01
Charge AND	0.17 \pm 0.02	0.06 \pm 0.01	0.32 \pm 0.03

Figure 11 shows how the inefficiency depends on the detection threshold in the case of *Charge AND*. The threshold is applied at each bar end.

6.3 Time resolution

The time resolution of bars L1, L2, and L4 was measured using the following procedure, repeated for each impact position of the beam along the bar.

As a first step, the charge samples from the SiPMs “left” (L) and “right” (R) with respect to the beam direction at the two bar ends were scanned in 0.5 ns steps, identifying a “start” time (t_L, t_R) as the first time bin corresponding to an ADC count greater than 10 with respect to the average baseline. An example of baseline-subtracted waveform is shown in Figure 12. The same procedure has been applied to the trigger signals, obtaining a t_0 for each event that was subtracted from t_L and t_R .

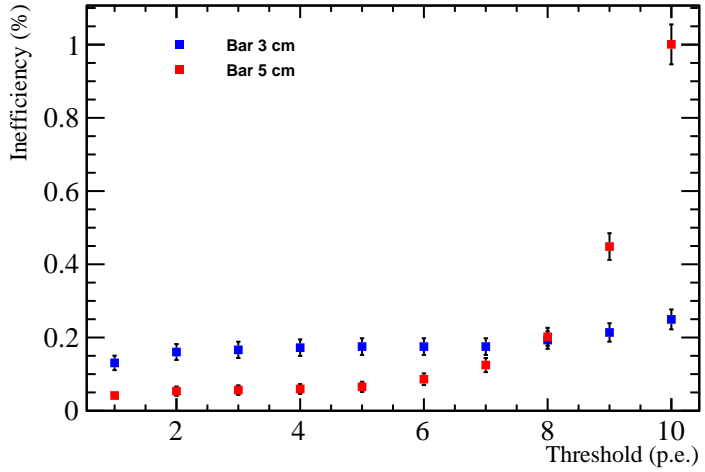


Figure 11. The inefficiency for 3 and 5 cm wide bars as a function of the charge detection threshold. The events are counted if the charge is over the specified threshold at each bar end.

As a second step, in order to compute the time-slewing corrections, the total charge $Q_{L,R}$ distributions were calculated, where $Q_{L,R}$ are the charges integrated over 350 ns starting at $t'_{L,R} = t_{L,R} - t_0$.

The $Q_{L,R}$ spectra were divided in 10 slices, each slice containing the same number of events, and for each slice a gaussian fit of the $t'_{L,R}$ distribution was done.

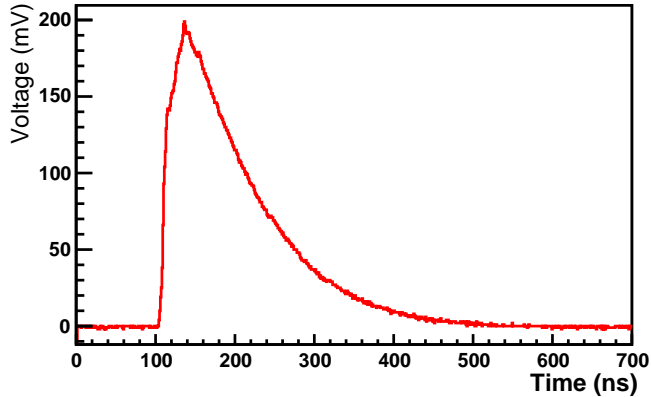


Figure 12. Example of baseline-subtracted waveform for 2 cm thick NICADD bars.

The average values of these fits, together with the corresponding values of $Q_{L,R}$, were used to find by linear interpolation a time-slewing correction term, as a function of $Q_{L,R}$, to be subtracted from the previous t'_L and t'_R , obtaining new “start” values $t''_{L,R} = t_{L,R} - t_0 - t_{L,R}^{\text{TS}}$. The values of $t''_{L,R}$ were histogrammed and gaussian fits were remade, this time for all charges $Q_{L,R}$ together. The averages of $t''_{L,R}$ as a function of the beam impact position measure the speed of light propagation along the fibre, and is shown in Figure 13 for bar L2.

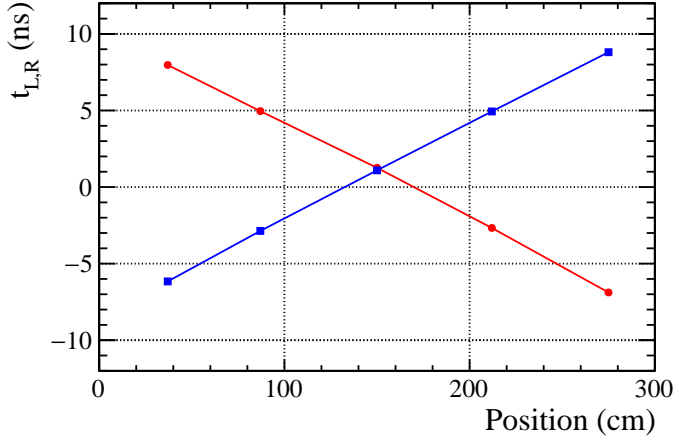


Figure 13. Speed of light propagation v_f in L2 fibre, for signals read by SiPM left (red line) and right (blue line); v_f is measured as (16.0 ± 0.1) cm/ns.

The time resolution for each bar as a function of the position of the beam along the fibre length was measured as the σ of a Gaussian function used to fit the time distributions of each SiPM individually and the sum of the two, using the relation $0.5 \cdot (t_L'' + t_R'')$. The results are shown in Figures 14, 15, 16 respectively for bars L1, L2 and L4.

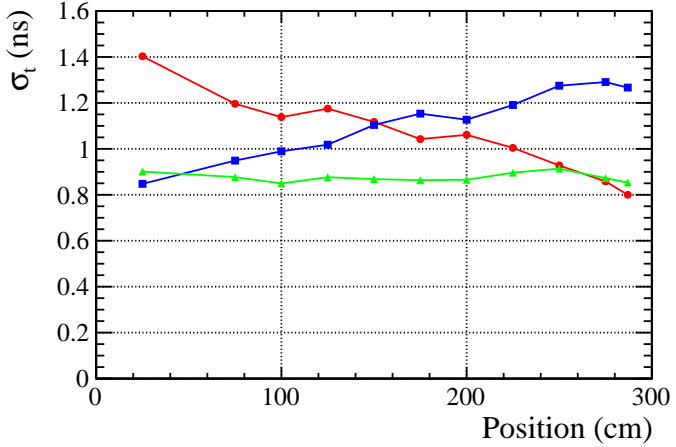


Figure 14. L1 bar time resolution using only SiPM $L(R)$, red circles(blue squares) and both SiPMs (green triangles).

From the point of view of the time resolution σ_t , the L2 bar provides the best results. The results obtained from bar L1, if still acceptable, would allow a great economy of scintillating material. For the L4 bar, with a 1.2 mm diameter fibre, the time resolution appears very marginal.

For completeness, we show in Table 6 the time resolution obtained in exactly the same way for short bars, read out only at one end, and with the beam impact point at 13 cm far apart from the photosensor.

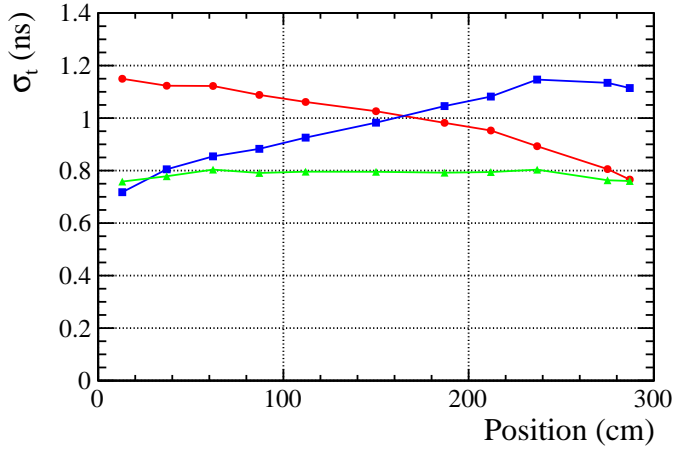


Figure 15. L2 bar time resolution using only SiPM $L(R)$, red circles(blue squares) and both SiPMs (green triangles).

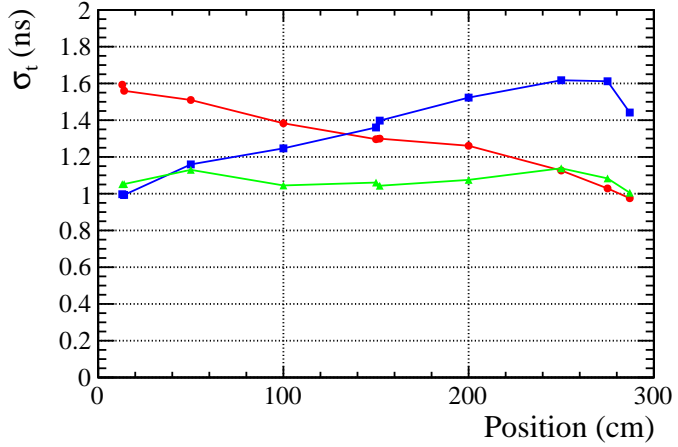


Figure 16. L4 bar time resolution using only SiPM $L(R)$, red circles(blue squares) and both SiPMs (green triangles).

Table 6. Time resolution for short bars S1, S2, S4, S5 and S8 defined in Table 1 when the beam impinges at ~ 13 cm with respect to the SiPM. Treatment of slewing corrections is the same described in the text for long bars L1–L4.

	time resolution [ns]
S1	0.756 ± 0.006
S2	0.676 ± 0.005
S4	0.820 ± 0.007
S5	0.676 ± 0.005
S8	0.730 ± 0.005

The measurement of the time resolution for Uniplast bars has been performed as follows. The waveform digitizer captures the pulse shape with steps of 200 ps each as shown in Figure 17. The typical pulse shape after the slow preamplifier is stretched over 1000 time samples, that correspond to 200 ns. The shoulder observed in the pulse is caused by the signal reflection in 2.5 m long twisted pair cable between MPPC and the preamplifier. The rise time of the pulse was used to obtain the timing mark of the event. The typical number of samples within the pulse front is over 60. This allows us to apply two different methods for calculating the timing, obtaining similar results.

The first method consists in fitting with straight lines the rising edge of the pulse shape and the baseline before the signal; the rising edge of the pulse shape is fitted between 5% and 85% of its maximum height. The crossing point of the lines gives the relative time coordinate. The method is illustrated in Figure 17.

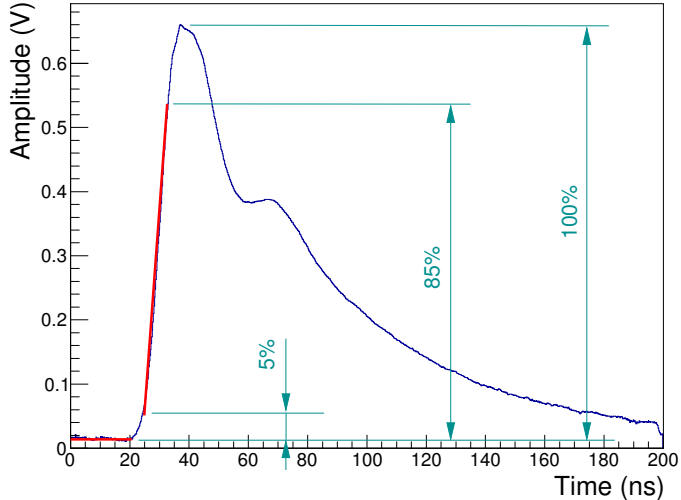


Figure 17. Fitting of digitized pulse shape to obtain the timing mark.

The time resolution was obtained by fitting with a Gaussian function the time distributions $0.5 \cdot (t''_R + t''_L)$ at different positions of the beam along the bar length.

The results for 3 and 5 cm wide bars are shown in Figure 18. The points are the average time resolution for the three tested bars of the same size. The average resolutions along the whole bar length are $\sigma_t = 724$ ps and $\sigma_t = 820$ ps for 3 and 5 cm wide bars, respectively.

The results for 10 cm bars are presented in Figure 19 (a) for the readout with two MPPCs (U4) and in Figure 19 (b) for the readout with four MPPCs (U3). The time resolution for the U4 and U3 bars were determined by fitting with a Gaussian function the distributions $(t''_L + t''_R) \cdot 0.5$ and $(t''_{1L} + t''_{1R} + t''_{2L} + t''_{2R}) \cdot 0.25$, respectively. We find $\sigma_t = 1.4$ ns for the bar readout by two MPPCs (U4) and $\sigma_t = 1$ ns for the bar read out by 4 MPPCs. The time resolution of the bar instrumented with four photosensors improves by $\sqrt{2}$, as expected.

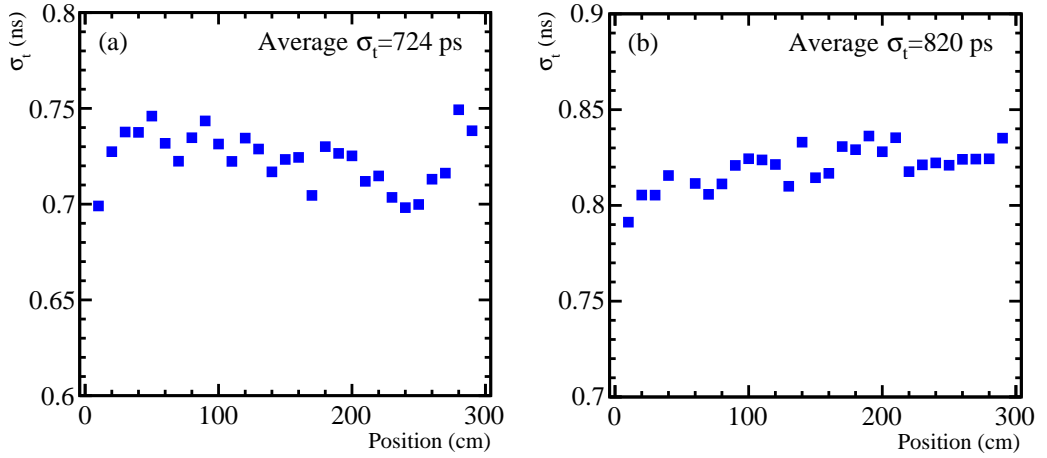


Figure 18. Time resolution for 3 cm (a) and 5 cm bars (b) vs position along the bars.

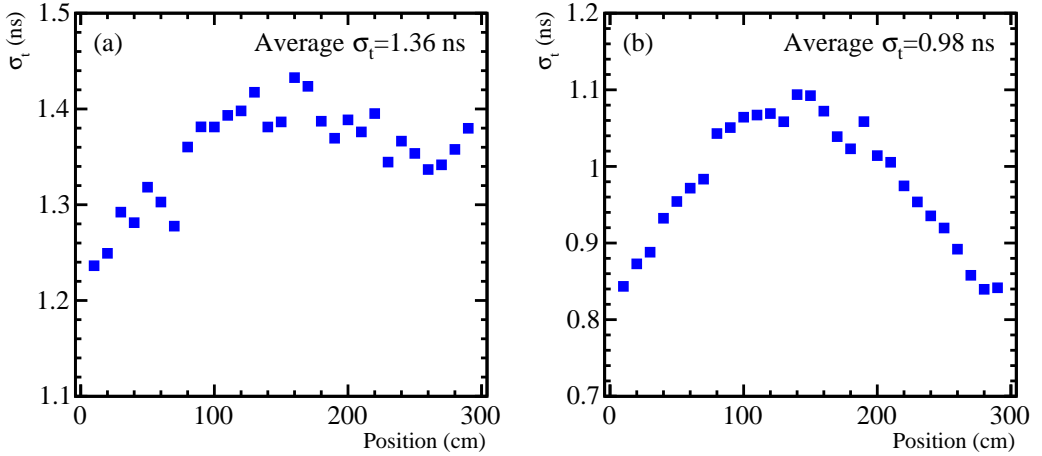


Figure 19. Time resolution for 10 cm bars with 2 MPPC readout (a) and 4 MPPC readout (b).

These results were obtained for the whole spectrum of pulse amplitudes. The time resolution of a single MPPC as a function of the light yield can be fitted as

$$\sigma_t = 6.6 \text{ ns} / \sqrt{L.Y.(p.e.)} - 0.14 \text{ ns}.$$

The second method to determine the time resolution consists in simulating the behaviour of a constant fraction discriminator on the pulse shape recorded by the digitizer. The time mark was fixed to the clock sample where the pulse amplitude exceeds the 15% fraction of the pulse height. The results were compatible with those obtained with the first method within the uncertainties.

7 Conclusions

Parameters as the light yield, time resolution and efficiency for minimum ionizing particles of different types of 300 cm and 25 cm long scintillating bars instrumented with wavelength shifting fibres and read out by different models of silicon photomultipliers have been measured at a test beam at the T9 area at the CERN Proton Synchrotron. A time resolution of 700-800 ps, constant along the bar length, and a light yield of \sim 140 (70) photoelectrons were obtained for the best prototypes 3 m long, 4.5 (5) cm wide and 2 (0.7 cm) thick. The detection efficiency for minimum ionizing particles exceeds 99.5% for the prototypes from UNIPLAST company. The results collected so far nicely match the requirements for the SHiP muon detector.

Acknowledgments

The authors would like to thank H. Wilkens, L. Gatignon, M. Jaeckel and R. Jacobsson for continuous support and help. This project has received funding from the European Union's Horizon 2020 research and innovation program under grant agreement No 654168. This work has been supported by the Grant #14-12-00560 of the Russian Science Foundation.

References

- [1] D. Michael et al., *The Magnetized steel and scintillator calorimeters of the MINOS experiment*, *Nucl. Instrum. Meth.* **A596**, (2008), 190.
- [2] K. S. McFarland, *MINERνA: A Dedicated neutrino scattering experiment at NuMI*, *Nucl. Phys. Proc. Suppl.* **159** (2006) 107. doi: 10.1016/j.nuclphysbps.2006.08.073.
- [3] T. Abe et al., *Belle II Technical Design Report* (2010).
- [4] K. Abe et al., *The T2K Experiment*, *Nucl. Instrum. Meth.* **A659** (2011) 106. doi: 10.1016/j.nima.2011.06.067.
- [5] M. Anelli et al., *SHiP Technical Proposal*, CERN-SPSC-2015-016, arXiv:1504.04956.
- [6] URL <http://nicadd.niu.edu/fnpl/>. FNAL NICADD Photoinjector Laboratory.
- [7] A. Pla-Dalmau, A. Bross, and K. Mellott, *Low-cost extruded plastic scintillator*, *Nucl. Instrum. Meth.* **A466** (2001) 482. doi: 10.1016/S0168-9002(01)00177-2.
- [8] Y. Kudenko, L. Littenberg, V. Mayatsky, O. Mineev, and N. Ershov, *Extruded plastic counters with WLS fibre readout*, *Nucl. Instrum. Meth.* **A469** (2001) 340. doi: 10.1016/S0168-9002(01)00780-X.
- [9] URL <http://www.detectors.saint-gobain.com/fibres.aspx>. Saint Gobain Crystals.
- [10] URL <http://kuraraypsf.jp/psf>. Kuraray Plastic Scintillating Fibres.
- [11] F. Acerbi et al., *NUV Silicon Photomultipliers With High Detection Efficiency and Reduced Delayed Correlated-Noise*, *IEEE transactions on Nuclear Science*, 62 (2015) 1318.
- [12] A. Ivashkin, Y. Kudenko, O. Mineev, and J. Imatato, *Scintillation ring hodoscope with WLS fibre readout*, *Nucl. Instrum. Meth.* **A394**, (1997), 321.
- [13] Y. Kudenko et al., *Nucl. Instr. Meth.* A469 (2001) 340.

- [14] http://www.eljentechnology.com/images/products/data_sheets/EJ-500.pdf
- [15] F. Hosomi et al., PoS PhotoDet2015 (2016) 046.
- [16] <http://advansid.com/products/product-detail/asd-rgb-nuv-3s-p>.
- [17] <http://advansid.com/products/product-detail/asd-rgb-nuv-1s-p>.